JOURNAL OF PROPULSION AND POWER
Vol. 12, No. 3, May–June 1996

Technical Notes

TECHNICAL NOTES are short manuscripts describing new developments or important results of a preliminary nature. These Notes cannot exceed 6 manuscript pages and 3 figures; a page of text may be substituted for a figure and vice versa. After informal review by the editors, they may be published within a few months of the date of receipt. Style requirements are the same as for regular contributions (see inside back cover).

Internal Ballistic Model for Spinning Star-Grain Motors

D. R. Greatrix*
Ryerson Polytechnic University,
Toronto, Ontario M5B 2K3, Canada

Introduction

A NORMAL or radial acceleration field can produce significant combustion rate augmentation in statically fired, spinning solid-propellant rocket motors (SRMs). The level of normal acceleration $\omega^2 r$ is dependent on motor spin rate ω and the surface-to-centerline distance r. Forward longitudinal acceleration in flight tends to counteract this increase in burning. In addition, noncylindrical grain cross sections (star, wagon-wheel, etc.) introduce appreciable lateral acceleration components relative to the local propellant surface, producing a similar reduction in peak acceleration effects. However, late into motor firings, where spin rate and radial distance may be approaching maximum levels, and the initial star or wagon-wheel grain shape in many cases are approaching a circular cross section, one may again encounter significant burning rate augmentation with normal acceleration.

Greatrix[1] has recently developed a phenomenological model for predicting normal, longitudinal, and lateral acceleration effects on solid-propellant combustion, and demonstrated some results for cylindrical-grain motors undergoing spinning and longitudinal acceleration with forward flight. In the present study, an evaluation of noncylindrical grain designs is undertaken, whereby lateral acceleration components with a varying peripheral contour may be included in the internal ballistics analysis. Simulated pressure-time histories for star-grain SRMs are presented to illustrate the effectiveness of the current modeling approach.

Model

The underlying concept of the phenomenological combustion model[1] is that the compression of the combustion zone, especially in the high-density, low-velocity region approaching the condensed-phase decomposition layer, is the dominant mechanism for burning rate augmentation under normal acceleration a_n. Compression relief with longitudinal or lateral sliding of evolving reactive fluid pockets or particles is represented by a displacement effect associated with the longitudinal or lateral acceleration component a_l, whereby one defines the acceleration vector orientation angle ϕ [i.e., $\tan^{-1}(a_l/a_n)$], with respect to the local propellant surface. The burning-rate model of Ref. 1 may be summarized as follows with the principal equation for overall burning rate r_b:

$$r_b = \frac{\beta(r_b + G_a/\rho_s)}{\exp[C_p\delta_0(\rho_s r_b + G_a)/k] - 1} \tag{1}$$

where the heat flux coefficient β correlates the enthalpy increase above (to flame temperature T_f) and below the burning propellant surface, and δ_0 is the reference energy film thickness for the combustion zone at a base burning rate r_0. The compressive effect of normal acceleration (coupled with pressure p) and the dissipative effect of longitudinal or lateral acceleration is stipulated through the accelerative mass flux G_a:

$$G_a = \frac{a_n p}{r_b}\frac{\delta_0}{RT_f}\frac{r_0}{r_b}\bigg|_{\phi=0^\circ}\cos^2\phi_d \tag{2}$$

where ϕ_d is the displacement or augmented orientation angle.[1] Note that a_n is assumed negative in value when directed into the propellant surface. Other combustion product properties such as gas thermal conductivity k, gas specific heat C_p, and specific gas constant R are given mean values representative of the combustion zone.

In considering a star-grain design, one has the complication of a varying burning rate with combined normal and lateral acceleration (and possibly longitudinal) in moving around the periphery at a given axial station. The inclination of the local propellant surface relative to the total acceleration vector will determine the local surface regression rate. One straightforward way of computing the local burning rate at a given time into a motor firing, and estimating the subsequent regression over a short time increment Δt, is to segment the core periphery section into a number of small linear elements (a similar approach may be found in Ref. 2). One need only consider a portion of a core periphery cross section because of symmetry with respect to the acceleration vector (e.g., a one-twelfth pie section for a six-pointed star).

With respect to the overall internal ballistics model, the equations of motion describing the quasisteady internal coreflow must be solved in conjunction with the pressure-dependent, coreflow-dependent, and acceleration-dependent components of the overall pyrolysis rate.[3] Given that the various burning-rate components are intrinsically coupled, an iterative solution procedure is generally required. The mean burning rate at a given axial position may be evaluated by summing the various burning rates around the periphery. To attain some level of accuracy, it is clear that a large number of elements must be selected at each core periphery location, in addition to setting an adequate number of axial segment positions along the motor grain. This is the computation penalty incurred in going from a cylindrical to a noncylindrical configuration.

Model Predictions and Discussion

Several SRMs of differing design were evaluated using the internal ballistic model described previously. Table 1 provides a list of the various motor test characteristics for two examples (A and B). Motor A has characteristics corresponding to the ALCOR IA motor as reported by Lucy.[4] The grain has a six-pointed star configuration, and propellant characteristics of an

Received May 11, 1995; presented as Paper 95-2876 at the AIAA/ASME/SAE/ASEE 31st Joint Propulsion Conference and Exhibit, San Diego, CA, July 10–12, 1995; revision received Nov. 16, 1995; accepted for publication Nov. 17, 1995.

*Assistant Professor, Department of Mechanical Engineering, 350 Victoria Street. Senior Member AIAA.

Table 1 Motor test characteristics

Motor	A	B
L_p, grain length, m	1.35	2.25
d_f, inner casing diameter, cm	51.1	34.0
d_t, nozzle throat diameter, cm	10.0	5.5
n, burn rate exponent	0.4	0.0
C, burn rate coefficient, cm/s/kPa^n	0.03	0.3
ρ_s, propellant density, kg/m^3	1750.0	1700.0
C_s, propellant specific heat, J/kg-K	1500.0	1350.0
T_f, K	2500.0	2400.0
T_s, propellant surface temperature, K	900.0	665.0
T_i, initial propellant temperature, K	294.0	294.0
C_p, J/kg-K	1900.0	1975.0
R, J/kg-K	378.0	396.0
k, W/m-K	0.17	0.17

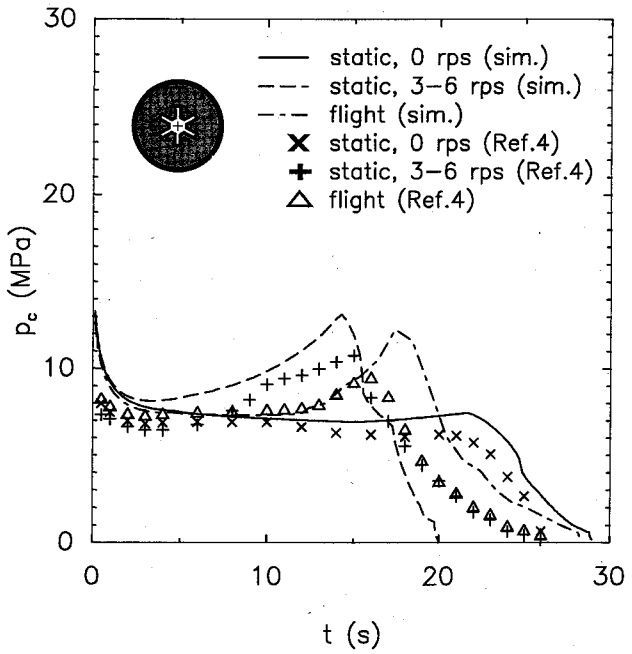

Fig. 1 Predicted pressure-time histories for static firing of motor A, with comparison to firing data of Ref. 4.

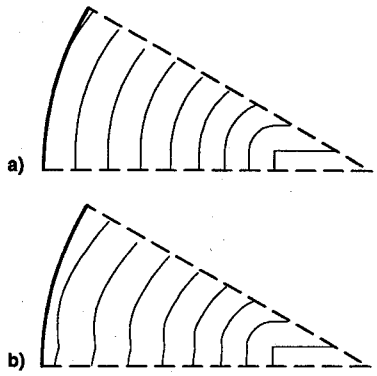

Fig. 2 Section grain profiles for motor A, static firing, a) without and b) with spinning, midlength axial station.

ammonium perchlorate/carboxyl-terminated polybutadiene (AP/CTPB) variant are assumed. Two predicted cases are illustrated in Fig. 1, with the corresponding firing data of Ref. 4, for the pressure-time history of the motor (static without spin and statically fired at a spin rate of 8 rps). The predicted results for both cases are qualitatively consistent with the reference data. Quantitatively, the base profile and the spin augmentation effect appears to be overpredicted somewhat, but because of a lack of available information, an exact correlation of all test characteristics was not attempted in setting up the simulation.

The grain cross-sectional profile at a midlength station is provided as a function of time in Figs. 2a and 2b (nonspinning periphery profile every 3 s and static spinning periphery profile every 3 s, respectively). For Fig. 2a, a series of clean profiles are produced with uniform burning around the periphery at a given time step. For Fig. 2b, the profiles are less clean with nonuniform burning, producing dips and rises with alternating strong and weak a_n effects coming into play, depending on the local surface inclination relative to the local acceleration vector orientation.

Motor B has characteristics corresponding to the NOTS 551-B motor as reported by Lucy.[4] The grain has a six-pointed star configuration and utilizes an aluminized ammonium perchlorate/polyurethane (AP/PU) composite propellant. Plateau-burning characteristics are assumed with this propellant (i.e., pressure-based burn-rate exponent $n \approx 0$), which has a high sensitivity to normal acceleration as is evidenced by the variable (3–6 rps over the course of the firing) static spinning motor curves of Fig. 3 in relation to the reference nonspinning case. The grain cross-sectional profile at a midlength station is provided as a function of time in Figs. 4a and 4b (nonspinning periphery profile every 4 s and static spinning periphery profile every 4 s, respectively). As before, Fig. 4a produces a series of clean profiles. For Fig. 4b, the profiles are considerably less

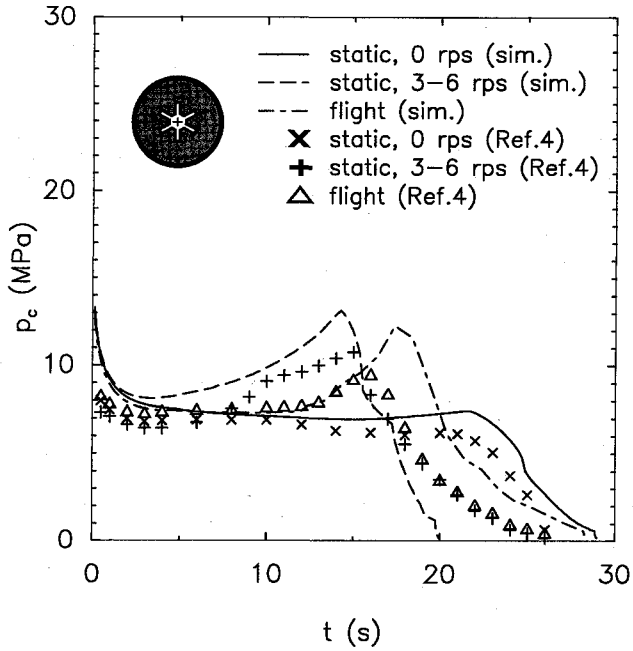

Fig. 3 Predicted pressure-time histories for static and in-flight firing of motor B, with comparison to firing data of Ref. 4.

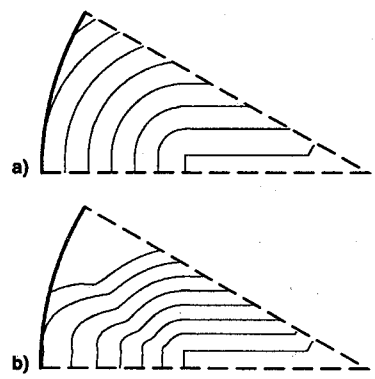

Fig. 4 Section grain profiles for motor B, static firing, a) without and b) with spinning, midlength axial station.

clean with nonuniform burning, with some pronounced dips and rises.

Overall, there is a good qualitative correlation between the predicted augmented pressure curve and the static firing data of Ref. 4. Because of nozzle throat erosion later in the experimental firing, the predicted peak pressure is somewhat higher than expected (no throat erosion modeled). Similarly, for the flight case with increasing forward acceleration and spin as the firing proceeds, the predicted pressure peaks somewhat higher than expected relative to the reported data of Ref. 4. Only later into the flight does the normal acceleration of the motor rotation begin to dominate the lateral and longitudinal acceleration components in affecting the combustion process.

References

[1]Greatrix, D. R., "Parametric Analysis of Combined Acceleration Effects on Solid-Propellant Combustion," *Canadian Aeronautics and Space Journal*, Vol. 40, No. 2, 1994, pp. 68–73.

[2]Hejl, R. J., and Heister, S. D., "Solid Rocket Motor Grain Burnback Analysis Using Adaptive Grids," *Journal of Propulsion and Power*, Vol. 11, No. 5, 1995, pp. 1006–1011.

[3]Greatrix, D. R., Gottlieb, J. J., and Constantinou, T., "Quasi-Steady Analysis of the Internal Ballistics of Solid-Propellant Rocket Motors," *Canadian Aeronautics and Space Journal*, Vol. 33, No. 2, 1987, pp. 61–70.

[4]Lucy, M. H., "Spin Acceleration Effects on Some Full-Scale Rocket Motors," *Journal of Spacecraft and Rockets*, Vol. 5, No. 2, 1968, pp. 179–183.

Propellant Design Relationships for Throttled Gas Generators

R. A. Frederick Jr.*
University of Alabama in Huntsville, Huntsville, Alabama 35899
and
Iwao Komai†
NOF Corporation, Taketoyo, Achii 470-23, Japan

Nomenclature

A_b = propellant burn surface area
a = burning rate coefficient
a' = burning rate coefficient at reference pressure and temperature
c^* = propellant characteristic exhaust velocity
K = burn area over throat area
$\dot{m}_f$ = mass flow rate of fuel
N_{MAX} = maximum allowable pressure sensitivity
n = pressure exponent
P = chamber pressure
P' = chamber pressure over reference pressure
r = propellant burn rate
T_i = initial propellant temperature
α = temperature sensitivity coefficient
α' = temperature sensitivity coefficient at reference pressure
ρ_p = propellant density

Subscripts
r = reference conditions
s = standard conditions
1 = maximum limit
2 = minimum limit

Received Aug. 25, 1994; revision received Nov. 2, 1995; accepted for publication Nov. 28, 1995.

*Assistant Professor, Department of Mechanical and Aerospace Engineering, Propulsion Research Center. Senior Member AIAA.

†Senior Research Engineer. Member AIAA.

Introduction

WHEN formulating gas generator propellants, the designer must achieve a specified mass flow schedule. One approach is to use propellants with large pressure sensitivity and a variable-area nozzle. This promotes substantial variations in mass flow while maintaining a reasonable pressure range. The propellant temperature sensitivity and combustion efficiency are additional factors that influence the design. The objective of this work is to calculate a propellant solution space that fulfills the design requirements for a variable-flow gas generator. The scope includes 1) developing a design methodology that incorporates mass flow rate, pressure, and temperature requirements; 2) deriving design equations for propellants with temperature-dependent pressure exponents; and 3) calculating regions of compliant propellant ballistics for an example ducted rocket application.

Approach

Gas Generator Constraints

The gas generator design is assumed to be bounded by mass flow rate, propellant temperature, and chamber pressure requirements. The mass flow rate range of a ducted rocket motor can be determined from anticipated altitude, flight Mach number, and operational oxidizer-to-fuel ratio considerations: $\dot{m}_{f1} \leq \dot{m}_f \leq \dot{m}_{f2}$. The gas generator must deliver this entire range. The operating environment dictates a range of initial propellant temperatures: $T_{i,1} \leq T \leq T_{i,2}$. The maximum chamber pressure is defined by structural/weight considerations of the missile. The minimum pressure could be guided by either the choked-flow or propellant extinguishment: $P_1 \leq P \leq P_2$. It is not required that this pressure range be spanned, but the pressure limits must not be violated.

For steady-state operation, the propellant burning rate range is derived from extreme values of the required mass flow rate and the propellant burn surface area by

$$r_2 = \dot{m}_{f\,\max}/\rho_p A_{b\,\min} \tag{1}$$

$$r_1 = \dot{m}_{f\,\min}/\rho_p A_{b\,\max} \tag{2}$$

A stable equilibrium chamber pressure also requires the pressure exponent must be less than one.

Figure 1 shows how these burn rate, pressure, and pressure-exponent limits form a parallelogram-shaped region (A–B–C–D) of compliant burn rate/pressure combinations. Initial temperature effects are illustrated by two propellant burn rate curves. The maximum temperature curve intersects point A, while the minimum temperature curve intersects point C. Expressing these design criteria mathematically, we have

$$r(P_1, T_2) \leq r_1 \quad \text{and} \quad r(P_2, T_1) \geq r_2 \tag{3}$$

and $n < 1$.

Mathematical Derivations

Propellant burning rate is assumed as a function of pressure and temperature with

$$r = a_s \exp[\alpha(T_i - T_{i,s})]P^{[n_s+\beta(T_i-T_{i,s})]} \tag{4}$$

Small variations in β will result in large changes in burning rate at operational pressures. Normalizing with a reference pressure P_r, at which the contribution of the β term is zero, yields,

$$r = a'_s \exp[\alpha'(T_i - T_{i,s})]P'^{[n_s+\beta(T_i-T_{i,s})]} \tag{5}$$